Chapter 17
An Iso-Geometric Analysis of Tow-Steered Composite Laminates: Free Vibration, Mechanical Buckling and Linear Flutter Analysis

S. Natarajan, S. M. Dsouza, A. L. N. Pramod, Hirshikesh, D. Adak, and K. Kamdi

1 Introduction

Layered materials belong to a new class of engineered materials that typically constitutes of two or more different phases separated by an interface. Due to different chemical and physical properties of the constituent materials, the material properties can be custom tailored to meet demanding low weight-to-strength ratio, improved corrosion and wear resistance [1–4]. Of the available composite materials, fiber reinforced composites are widely studied. This is because, in fiber laminated composites, the fiber volume fraction can be controlled when compared to other composites, such as particle or filament refined composites. Until recently, fiber laminated composites are made up of straight fibers that are homogeneously distributed within a lamina. The macroscopic properties are improved by the constituents mechanical properties, the stacking sequence and thickness of each ply and fiber angle within a lamina. As the fiber angle is constant within a ply, these are also referred to as constant stiffness laminated composites. This has led the researchers to focus on improving the effective property. Thanks to the recent advances in manufacturing, stiffness can now be varied within a lamina [5, 6]. There are many approaches to achieve stiffness variation within a lamina. A few among them are by: (a) changing the fiber angle within a lamina (i.e., use curvilinear fiber) [7–9]; (b) changing the volume fraction of fibers [10, 11]; (c) addition or dropping of plies to the laminates [12, 13] and (d) attaching discrete stiffeners to the laminates. Amongst them, lamina with spatially changing fiber angle is advantageous because, continuous change in fiber orientation avoids sudden change in the thickness which could be a cause for stress concentrations [14]. As the angle of the fiber in the lamina depends on the spatial coordinate and the tow-placement machines control the fiber placement, they are called as tow-steered composite laminates (TSCL).

S. Natarajan (✉) · S. M. Dsouza · A. L. N. Pramod · Hirshikesh · D. Adak · K. Kamdi
Department of Mechanical Engineering, Indian Institute of Technology Madras, Chennai, India
e-mail: snatarajan@iitm.ac.in

S. Sahoo (ed.), *Recent Advances in Layered Materials and Structures*,
Materials Horizons: From Nature to Nanomaterials,
https://doi.org/10.1007/978-981-33-4550-8_17

Composite materials with varying stiffness has received considerable interest amongst researchers and practising engineers, as they may lead to lean design [15–18]. As early as 1990, Hyer and Lee [15] introduced a novel technique to improve the structural response of panels with cutouts by changing the stiffness of the panel in the lamina. Although, the concept of tailored composite was developed two decades back, only recently there is a surge in interest in understanding the response of two-steered composites [19–24]. This can be possible, thanks to the recent advances in manufacturing capability that has made tow-steered composite laminates a reality [25–27]. For TSCL plates, the stiffness coefficients are functions of spatial coordinates as the angle of the fiber is continuously changing. Apart from this, they also exhibit variable bending and coupling stiffness. This can be advantages as a varying fiber angle within a lamina can lead to altered loading paths with improved load carrying capacity. Different plate theories, such as classical plate theory and other shear deformation plate theories to study the response of tow-steered laminated composites. Honda and Narita [28] studied the natural frequencies of laminates with curvilinear paths using classical plate theory. Coburn et al. [29] used the first order shear deformation theory numerically studied the influence of varying fiber angle on the critical buckling load of TSCL panel by generalized Rayleigh-Ritz procedure. The third order shear deformation theory was adopted in the work of Akhavan and coworkers [20, 23, 24] to study both the dynamic and the static response of moderately thick and thin tow-steered composite plates. Their study concluded that the influence of tow-steered fibers are more pronounced in thin plates than thick plates. Aforementioned studies employed either Lagrange based finite elements and/or meshfree approaches and studied the global response of tow-steered composite plates.

In this chapter, vibration, mechanical buckling and linear flutter analysis of tow-steered composite laminates is studied using an iso-geometric analysis framework. Reissner-Mindlin plate theory is used for describing the displacement field and basis splines for spatial discretization. The chapter is organized as follows: an overview of plate theory is presented in Sect. 2, followed by a brief discussion on isogeometric analysis framework in Sect. 3. The section also discussed a numerical procedure to alleviate shear locking syndrome. Section 4 presents numerical results for tow-steered composite laminates, followed by conclusions.

2 Theoretical Formulation

Reissner and Mindlin theory (RMT), an improvement of the CLT to model moderately thick and relatively thin plate. The salient feature of this theory when compared to CLPT is that the through thickness distribution is assumed to be linear. In this section, we present an overview of the RMT and develop the corresponding weak form based on a Galerkin procedure. Figure 1 shows a representation of a three layered plate with a, b as in-plane dimensions and h representing the total plate thickness. The plate aspect ratio is $\frac{a}{b}$ and $\frac{a}{h}$ defines the thickness ratio. Here, only

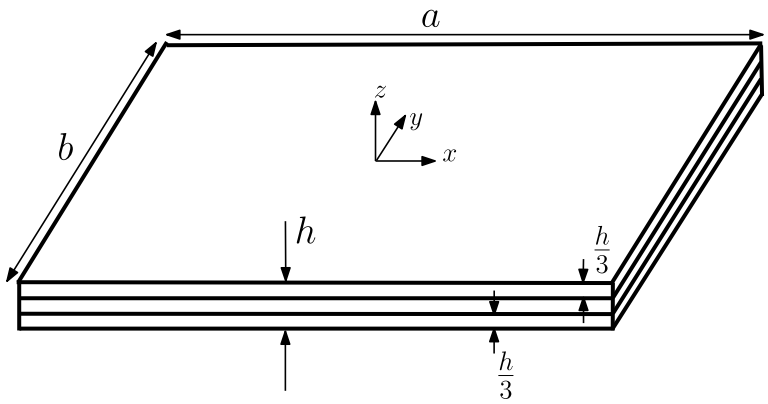

Fig. 1 Composite Laminate plate, a, b and h represents the in-plane dimensions and the total thickness of the plate, respectively

the midplane of the plate occupying an open domain $\Omega \subset \mathbb{R}^2$, with boundary Γ and unit outward normal, $\mathbf{n}$ is considered. The boundary of plate is assumed to accommodate the decompositions over which Dirichlet and Neumann boundary conditions are specified. Any point, P on the plate is represented by a triplet (x, y, z).

Let u_o, v_o, w_o represent the midplane displacements of the plate and β_x and β_y the rotations along x and y axis. The global displacements u, v, w are written in terms of the midplane displacements and rotations as:

$$\begin{pmatrix} u(\mathbf{x},t) \\ v(\mathbf{x},t) \\ w(\mathbf{x},t) \end{pmatrix} = \begin{pmatrix} u_o(x,y,t) \\ v_o(x,y,t) \\ w_o(x,y,t) \end{pmatrix} + z \begin{pmatrix} \beta_x(x,y,t) \\ \beta_y(x,y,t) \\ 0 \end{pmatrix} \tag{1}$$

where $\mathbf{x} = (x, y, z)$. The small strain tensor in vector form is expressed in terms of the displacements by:

$$\boldsymbol{\varepsilon} = \begin{Bmatrix} \varepsilon_{xx} \\ \varepsilon_{yy} \\ 2\varepsilon_{xy} \\ 2\varepsilon_{xz} \\ 2\varepsilon_{yz} \end{Bmatrix} = \begin{Bmatrix} \dfrac{\partial u_o}{\partial x} \\ \dfrac{\partial v_o}{\partial y} \\ \dfrac{\partial u_o}{\partial y} + \dfrac{\partial v_o}{\partial x} \\ \dfrac{\partial w_o}{\partial x} + \beta_x \\ \dfrac{\partial w_o}{\partial y} + \beta_y \end{Bmatrix} + z \begin{Bmatrix} \dfrac{\partial \beta_x}{\partial x} \\ \dfrac{\partial \beta_y}{\partial y} \\ \dfrac{\partial \beta_x}{\partial y} + \dfrac{\partial \beta_y}{\partial x} \\ 0 \\ 0 \end{Bmatrix} \tag{2}$$

The above strain-displacement relation in terms of the mid-plane strain $\boldsymbol{\varepsilon}_p$, bending strain $\boldsymbol{\varepsilon}_b$ and shear strain $\boldsymbol{\varepsilon}_s$ as:

$$\boldsymbol{\varepsilon} = \begin{Bmatrix} \boldsymbol{\varepsilon}_p \\ \mathbf{0} \end{Bmatrix} + \begin{Bmatrix} z\boldsymbol{\varepsilon}_b \\ \boldsymbol{\varepsilon}_s \end{Bmatrix} \tag{3}$$

where

$$\boldsymbol{\varepsilon}_p = \begin{Bmatrix} \dfrac{\partial u_o}{\partial x} \\ \dfrac{\partial v_o}{\partial y} \\ \dfrac{\partial u_o}{\partial y} + \dfrac{\partial v_o}{\partial x} \end{Bmatrix}, \quad \boldsymbol{\varepsilon}_b = \begin{Bmatrix} \dfrac{\partial \beta}{\partial x} \\ \dfrac{\partial \beta}{\partial y} \\ \dfrac{\partial \beta}{\partial y} + \dfrac{\partial \beta}{\partial x} \end{Bmatrix}, \quad \boldsymbol{\varepsilon}_s = \begin{Bmatrix} \beta_x + \dfrac{\partial w}{\partial x} \\ \beta_y + \dfrac{\partial w}{\partial y} \end{Bmatrix} \tag{4}$$

The membrane stress resultants $\mathbf{N}$ and the bending stress resultants $\mathbf{M}$ can be related to the membrane strain $\boldsymbol{\varepsilon}_p$ and bending strain $\boldsymbol{\varepsilon}_b$ through the following relation [30]:

$$\begin{aligned} \mathbf{N} &= \begin{Bmatrix} N_{xx} \\ N_{yy} \\ N_{xy} \end{Bmatrix} = \mathbf{A}\boldsymbol{\varepsilon}_p + \mathbf{B}\boldsymbol{\varepsilon}_b \\ \mathbf{M} &= \begin{Bmatrix} M_{xx} \\ M_{yy} \\ M_{xy} \end{Bmatrix} = \mathbf{B}\boldsymbol{\varepsilon}_p + \mathbf{D}_b\boldsymbol{\varepsilon}_b \end{aligned} \tag{5}$$

where the extensional coefficients $\mathbf{A} = A_{ij}$, bending-extensional coefficients $\mathbf{B} = B_{ij}$ and bending coefficient $\mathbf{D}_b = D_{ij}$ $(i, j = 1, 2, 6)$ are given by:

$$\{A_{ij}, B_{ij}, D_{ij}\} = \int_{-h/2}^{h/2} \overline{Q}_{ij}\{1, z, z^2\}\mathrm{d}z \tag{6}$$

The transverse shear force, $\{Q_{xz}, Q_{yz}\}$ and the transverse shear strain, $\boldsymbol{\varepsilon}$ are related by:

$$\begin{aligned} Q_{xz} &= K_s \int_{-h/2}^{h/2} \sigma_{xz}\mathrm{d}z = K_s\overline{Q}_{55}(\beta_x + w_{0,x}) \\ Q_{yz} &= K_s \int_{-h/2}^{h/2} \sigma_{yz}\mathrm{d}z = K_s\overline{Q}_{44}(\beta_y + w_{0,y}) \end{aligned} \tag{7}$$

with K_s the shear correction factor, $\overline{Q}_{ij}$ in the above equations are called as the global stiffness coefficients that depend on the local stiffness coefficients, which in turn depends on the fiber orientation within the ply. The first element of $\overline{Q}$, i.e., $\overline{Q}_{11}$ is given by:

$$\overline{Q}_{11} = Q_{11}\cos(T(x))^4 + Q_{12}\sin(T(x))^4 + 2(Q_{12} + 2Q_{33})\left[\cos(T(x))^2\sin(T(x))\right]^2 \tag{8}$$

$T(x)$ is the fiber angle in a lamina. In present study, angle within the fiber is a continuous function of the position and is given by:

$$T(x) = T0 - \frac{(T1 - T0)}{a/2}\text{abs}(x), \quad x = \pm a/2 \tag{9}$$

where $T0$ is the angle of the fiber at the center of the plate and $T1$ at the edge. The orientation of the fiber for the k^{th} layer is then represented as $< T0^k|T1^k >$ (see Fig. 2). Theoretically, the fiber can take any value between $-90°$ and $90°$, however, manufacturing difficulties dictate that certain orientations lead to larger curvature that can cause fiber breakage during tow placement [31]. To ensure that the local curvature does not exceed a critical value and that is feasible from a manufacturing guidelines, the following relation is employed:

$$\kappa(x) = -\frac{(T0 - T1)}{a/2}\cos\left(T0 - (T0 - T1)\frac{x}{a/2}\right) < \frac{82}{25} \tag{10}$$

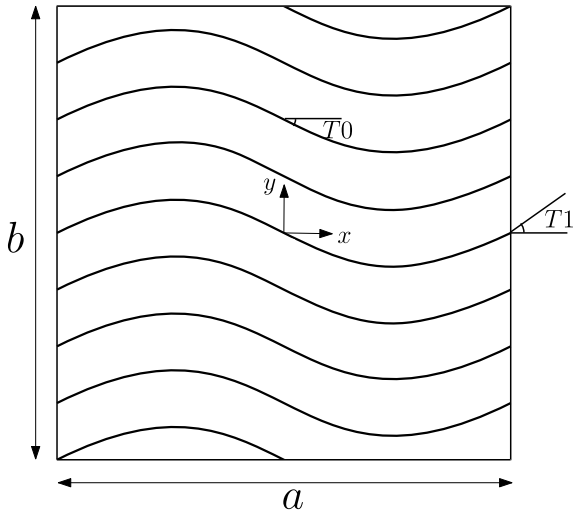

Fig. 2 Geometry of the plate and a representation of tow-steered fibers. The angle is measured in the anti-clockwise direction from the positive x-axis

The local stiffness coefficients, Q_{ij} are given by:

$$\begin{bmatrix} Q_{11} & Q_{12} & Q_{16} \\ Q_{12} & Q_{22} & Q_{26} \\ Q_{16} & Q_{26} & Q_{66} \end{bmatrix} = \begin{bmatrix} \dfrac{E_1}{1-\nu_{12}\nu_{21}} & \dfrac{\nu_{12}E_2}{1-\nu_{12}\nu_{21}} & 0 \\ \dfrac{\nu_{12}E_2}{1-\nu_{12}\nu_{21}} & \dfrac{E_2}{1-\nu_{12}\nu_{21}} & 0 \\ 0 & 0 & G_{12} \end{bmatrix} \tag{11}$$

and $Q_{44} = G_{23}$ and $Q_{55} = G_{13}$. The local fiber direction and the direction perpendicular to it is denoted by subscripts '1' and '2', respectively. This is measured within the plane of the lamina. The local stiffness coefficients, defined at the ply (or lamina) level are transformed to global coordinates by a simple coordinate transformation. In the present study, due to the curvilinear fibers, the coefficient matrices are functions of spatial direction, x. With the above definitions, the strain energy U, the kinetic energy T, externally applied forces V of the composite plate can be written as:
Strain energy:

$$\begin{aligned} U(\boldsymbol{\delta}) &= \frac{1}{2}\int_{\Omega} \{\boldsymbol{\varepsilon}_p^{\mathrm{T}}\mathbf{N} + \boldsymbol{\varepsilon}_b^{\mathrm{T}}\mathbf{M} + \boldsymbol{\varepsilon}_s^{\mathrm{T}}\mathbf{Q}\}\,\mathrm{d}\Omega \\ &= \frac{1}{2}\int_{\Omega} \{\boldsymbol{\varepsilon}_p^{\mathrm{T}}\mathbf{A}\boldsymbol{\varepsilon}_p + \boldsymbol{\varepsilon}_p^{\mathrm{T}}\mathbf{B}\boldsymbol{\varepsilon}_b + \boldsymbol{\varepsilon}_b^{\mathrm{T}}\mathbf{B}\boldsymbol{\varepsilon}_p + \boldsymbol{\varepsilon}_b^{\mathrm{T}}\mathbf{D}\boldsymbol{\varepsilon}_b + \boldsymbol{\varepsilon}_s^{\mathrm{T}}\mathbf{E}\boldsymbol{\varepsilon}_s\}\mathrm{d}\Omega \end{aligned} \tag{12}$$

Kinetic energy:

$$T(\boldsymbol{\delta}) = \frac{1}{2}\int_{\Omega} \{I_0(\dot{u}_0^2 + \dot{v}_0^2 + \dot{w}_0^2) + I_1(\dot{\theta}_x^2 + \dot{\theta}_y^2)\}\mathrm{d}\Omega \tag{13}$$

Work done due to externally applied forces

$$V(\boldsymbol{\delta}) = \int_{\Omega} N_x\left(\frac{\partial u_z}{\partial x}\right)^2 + N_y\left(\frac{\partial u_z}{\partial y}\right)^2 + 2N_{xy}\left(\frac{\partial u_z}{\partial x}\right)\left(\frac{\partial u_z}{\partial y}\right)\mathrm{d}\Omega \tag{14}$$

where $\boldsymbol{\delta} = \{u_o, v_o, w_o, \beta_x, \beta_y\}$ is the nodal degrees of freedom associated to the displacement field in finite element discretization, $I_0 = \int_{-h/2}^{h/2} \rho \mathrm{d}z$ and $I_1 = \int_{-h/2}^{h/2} z^2 \rho \mathrm{d}z$, ρ is the mass density. In addition, in the case of plate immersed in a supersonic flow, the work done by the fluid (non-conservative) should be accounted for, which is given by:

$$W(\boldsymbol{\delta}) = \int_{\Omega} \Delta p\, w\, \mathrm{d}\Omega \tag{15}$$

where Δp is the aerodynamic pressure, which in this study is based on first-order piston theory:

$$\Delta p = \frac{\rho_a U_a^2}{\sqrt{M_\infty^2 - 1}} \left[\frac{\partial w}{\partial x} \cos \Psi + \frac{\partial w}{\partial y} \sin \Psi \right] \tag{16}$$

where ρ_a, U_a, M_∞ and Ψ are the free stream air density, velocity of air, Mach number and flow angle, respectively. The governing equations of motion for: (a) free vibration and (b) mechanical buckling are obtained by writing the Lagrange equations of motion given by:

$$\left[\frac{\partial(-V - U + T)}{\partial \dot{\delta}_i} \right]_{,t} - \left[\frac{\partial(-V - U + T)}{\partial \delta_i} \right] = 0, \quad i = 1, 2, \cdots, n \tag{17}$$

Free vibration To get the finite element equation, we substitute Eqs. (12) and (13) in Eq. (17) and follow standard Galerkin procedure to get:

$$\mathbf{K}\boldsymbol{\delta} + \mathbf{M}\ddot{\boldsymbol{\delta}} = \mathbf{0} \tag{18}$$

where $\mathbf{M}$ is the consistent mass matrix and the following algebraic equation is obtained upon replacing $\ddot{\boldsymbol{\delta}} = \omega^2 \boldsymbol{\delta}$

$$(-\omega^2 \mathbf{M} + \mathbf{K})\boldsymbol{\delta} = 0 \tag{19}$$

where ω is the eigenvalue of the system, also known as the frequency.

Buckling In case of buckling, the discretized equations are obtained upon substituting Eqs. (12) and (14) into Eq. (17):

$$\left[\mathbf{K} - N^{\text{cr}} \mathbf{K}_G\right] \boldsymbol{\delta} = \mathbf{0} \tag{20}$$

where N^{cr} is the buckling load and $\mathbf{K}_G$ is the geometric stiffness matrix that depends on the residual stress. The residual stress state in turn depends on the ply lay-up. To estimate the stress state, for an assumed mechanical load, a pre-buckling displacement field is obtained by solving a static bending problem. Then the geometric stiffness matrix is computed using this stress state. The critical buckling load, N^{cr} is then obtained by solving Eq. (20) using standard eigen routines.

Linear flutter For linear flutter analysis, the Lagrange equations of motion is rewritten after introducing the contribution due to the non-conservative load as:

$$\left[\frac{\partial(-U + W + T)}{\partial \dot{\delta}_i} \right]_{,t} - \left[\frac{\partial(-U + W + T)}{\partial \delta_i} \right] = 0, \quad i \in (1, n) \tag{21}$$

Similar to free vibration and buckling, the finite element equations are obtained by following the Galerkin procedure and is given by:

$$(\mathbf{K} + \lambda \mathbf{K}_{\text{aero}})\, \boldsymbol{\delta} + \mathbf{M}\ddot{\boldsymbol{\delta}} = \mathbf{0} \tag{22}$$

The characteristic of the time function, $\ddot{\boldsymbol{\delta}} = -\omega^2\boldsymbol{\delta}$ is substituted to yield the following equation:

$$\left[-\omega^2\mathbf{M} + \left(\mathbf{K} + \frac{\rho_a U_a^2}{\sqrt{M_\infty^2 - 1}}\mathbf{K}_{\text{aero}}\right)\right]\boldsymbol{\delta} = \mathbf{0} \tag{23}$$

where $\mathbf{K}_{\text{aero}}$ represents the contribution due to the aerodynamic force, When $\frac{\rho_a U_a^2}{\sqrt{M_\infty^2 - 1}} = \lambda = 0$, the system is positive definite and hence $\omega \in \mathbb{R}$. The addition of the aerodynamic matrix to the stiffness matrix, makes the resulting matrix unsymmetric and leads to complex eigenvalue problem when $\lambda > 0$. This is because $\mathbf{K}_{\text{areo}}$ is unsymmetric. As λ is increased monotonically, for a particular pressure, two eigenmodes coalesce and the corresponding eigenvalue becomes complex conjugates. The critical value of the pressure at which the eigenvalue becomes complex conjugates is called the critical aerodynamic pressure, λ_{cr} and upon further increase, the system is unstable.

3 Overview of Iso-Geometric Analysis

This study employs the non-uniform rational basis spline (NURBS) as trial and test functions to represents the geometry and to approximate the unknown field variables within a finite element framework. This is in contrast to the conventional Lagrange type finite elements, where Lagrange polynomials represent the unknown fields and the domain. Introduced and coined as Iso-geometric analysis (IGA) by Hughes and co-workers [32, 33], the IGA has been applied to wider problems. Some of the salient features include: (a) higher continuity of the basis functions (b) exact representation of the geometry within the FE model and (c) seamless link between the CAD and the FEA.

The following information is required to define a B-spline basis functions:

- control points, P_i;
- knot vector, Ξ, a set of parametric values arranged in ascending sequence, $\xi_i \leq \xi_{i+1}, i = 0, 1, \ldots, m-1$;
- the degree of the curve p.

With this information, the B-spline basis function, $N_{i,p}$ of degree p is given by a recurrence relation:

$$N_{i,0}(\xi) = \begin{cases} 1 \text{ if } \xi_i \leq \xi \leq \xi_{i+1} \\ 0 \quad \text{otherwise} \end{cases}$$

$$N_{i,p}(\xi) = \frac{\xi - \xi_i}{\xi_{i+p} - \xi_i} N_{i,p-1}(\xi) + \frac{\xi_{i+p+1} - \xi}{\xi_{i+p+1} - \xi_{i+1}} N_{i+1,p-1}(\xi) \tag{24}$$

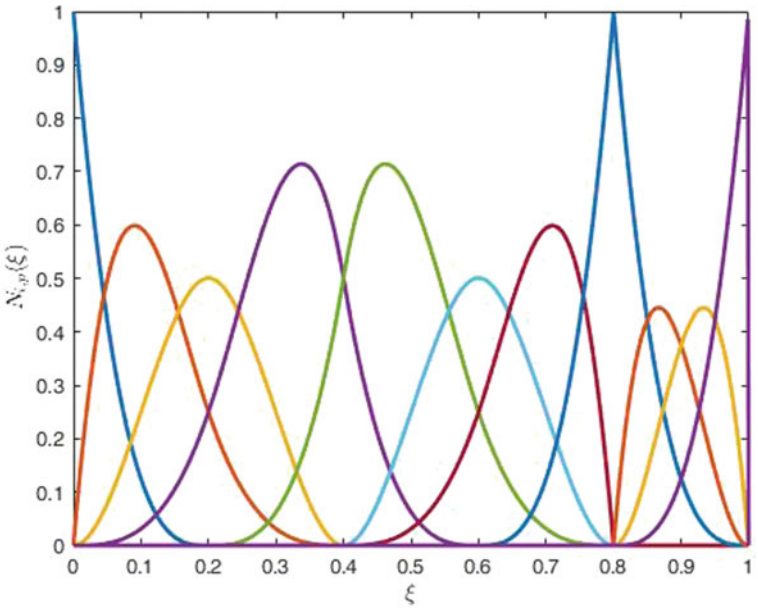

Fig. 3 B-splines for order of the curve, $p = 3$

If each of the control point has an associated weight defined, then the B-splines are termed as non-uniform rational B-splines. A pth degree NURBS curve is written as:

$$\mathbf{C}(\xi) = \frac{\sum_{i=0}^{m} N_{i,p}(\xi) w_i \mathbf{P}_i}{\sum_{i=0}^{m} N_{i,p}(\xi) w_i} \tag{25}$$

Figure 3 shows the fourth order B-splines with a knot vector,

$$\Xi = \{0, 0, 0, 0, 0.2, 0.4, 0.4, 0.6, 0.8, 0.8, 0.8, 1, 1, 1, 1\}$$

.

The important characteristics of NURBS basis functions is that it has all the necessary properties that a Galerkin framework requires, i.e., (i) the basis functions are positive everywhere within the span, (ii) sum of the basis functions is unity; (iii) interpolatory at the end points. Further the key advantage is that the geometry is exactly represented, as the same function is used to describe the geometry. One of the attractive features of these functions is that the continuity can be adapted to the specific needs of the problem. Typically, these are one-dimensional functions and a surface is presented by a tensor product of such one-dimensional functions with

separate knot vectors in each of the parametric dimensions (similar to the case of Lagrange type finite elements) given by:

$$\mathbf{C}(\xi, \eta) = \sum_{i=1}^{n} \sum_{j=1}^{m} N_{i,p}(\xi) M_{j,q}(\eta) \mathbf{P}_{i,j} \tag{26}$$

where $\mathbf{P}_{i,j}$ represents the coordinates of the control net and $N_{i,p}$ and $M_{j,q}$ are the unidirectional B-spline basis functions defined on the knot vectors. With this definition, a NURBS surface can be written as:

$$\mathbf{C}(\xi, \eta) = \frac{\sum_{i=1}^{n} \sum_{j=1}^{m} N_{i,p}(\xi) M_{j,q}(\eta) \mathbf{P}_{i,j} w_i w_j}{w(\xi, \eta)} \tag{27}$$

where $w(\xi, \eta)$ represents the weighting function. The vector of nodal unknowns $\boldsymbol{\delta}$ within the control mesh is approximated by:

$$\boldsymbol{\delta} = \sum_{J} \mathbf{C} \boldsymbol{\delta} \tag{28}$$

Figure 4 shows a representative geometry of the plate and a control net. As seen earlier, the Mindlin theory includes transverse shear deformations and the following condition must be satisfied if Mindlin plate theory is employed to study thin plates:

$$\nabla w + \theta = 0 \tag{29}$$

which states that the shear strain vanishes as the plate becomes thinner. However, when applied to thin plates the NURBS basis functions suffer from shear locking. In this chapter, we employ an artificial shear correction factor introduced by Kikuchi and Ishii [34] originally for 4-noded bilinear element to alleviate the shear locking syndrome, given by:

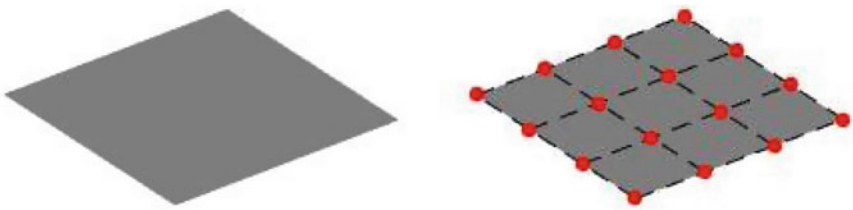

Fig. 4 **a** Plate represented using the NURBS basis functions $p = 3$, with the knot vector, $\Xi = \{0, 0, 0, 0, 1, 1, 1, 1\}$ in both the spatial directions. **b** Red dots indicate the control points and the black dashed lines represent the control mesh

$$K_s^e = K_s \frac{\left(\frac{h}{\beta l_e}\right)^2}{\left(1 + \left(\frac{h}{\beta l_e}\right)^{2n}\right)^{1/n}}, \quad n, \beta \in \mathbb{Z}^+ \tag{30}$$

where l_e is the diameter of the element.

4 Results

In this section, using the IGA framework, we numerically study the free vibration, mechanical buckling and flutter analysis of tow-steered laminated composites. The effect of the following parameters are considered on the output characteristics whilst discussing the results: plate thickness, number of plies and angle of the fiber within the lamina. For all the examples, it is assumed that all layers are of equal thickness and the angle of the fiber is measure with respect to $x-$ axis. In all the cases, cubic NURBS are employed, unless mentioned otherwise. The following Dirichlet conditions are considered for the present study:
Clamped edges:

$$u_o = v_o = w_o = \beta_x = \beta_y = 0 \quad \text{on} \quad x = 0, a \quad \& \quad y = 0, b$$

Simply supported edges:

$$u_o = w_o = \beta_y = 0 \quad \text{on} \quad x = 0, a; \quad v_o = w_o = \beta_x = 0 \quad \text{on} \quad y = 0, b$$

4.1 Free Vibration

Before presenting the results from the present framework, the results from the developed formulation is compared against results in the literature. For this study, 4-layered cross-ply laminated composites with $h = 0.2$ and straight fibers, i.e., $T1 \equiv T0$ are considered. The material properties are: $E_1/E_2 = 10, 40$, $G_{12} = G_{13} = 0.6E_2$, $G_{23} = 0.5E_2$, $\nu_{12} = 0.25$, $\rho = 1$ and $E_2 = E_3$. Table 1 compares the normalized frequency, $\overline{\omega} = \omega \frac{a^2}{h}\sqrt{\frac{\rho}{E_2}}$ from the present framework with that of results in [35, 36]. It is inferred that with mesh refinement the solution converges and yield comparable results. For subsequent discussions, a control mesh of 20×20 with cubic NURBS is employed.

Table 1 First non-dimensionalized frequency $\overline{\omega}$ for a 4-layered cross-ply laminates with $h = 0.2$

Method	Mesh size	$\frac{E_1}{E_2}$	
		10	40
IGA	3× 3	8.1286	10.4800
	5 × 5	8.2355	10.7140
	10 ×10	8.2823	10.8184
	20 ×20	8.2942	10.8450
Ref. [36]		8.2924	10.8490
Ref. [35]		8.2982	10.8540

Table 2 First five fundamental frequency, ω (rad/s) for TSCL. The edges are simply supported

Ref. [14]	IGA			
	10 × 10	20 × 20	30 × 30	$\%\Delta_{30\times30}$
309.1	315.0	309.9	309.1	0.0136
503.3	530.5	509.3	505.9	0.5245
852.1	954.0	867.4	854.3	0.2627
1143.5	1203.4	1144.0	1134.3	0.8053
1297.3	1416.1	1324.8	1296.2	0.0805

Next, the results from the present framework are compared for tow-steered composite laminates. In this case, the laminated plate is consists of three layers with ply configuration:

$$\langle 30^\circ, 0^\circ\rangle, \langle 45^\circ, 90^\circ\rangle, \langle 30^\circ, 0^\circ\rangle$$

The plate thickness, $h = 0.01$ and the material properties are: (E_1, E_2, G_{12}, G_{13}, G_{23}, ν_{12}, ν_{13}, ν_{23}) = (173 GPa, 7.2 GPa, 7.2 GPa, 3.76 GPa, 3.76 GPa, 3.76 GPa, 0.29, 0.29, 0.29) and $\rho = 1540\,\mathrm{kg/m^3}$ are used for the study. The numerical convergence of the first five fundamental frequencies are presented in Table 2.

First, the free vibration characteristics of TSCL is studied. Two-layered anti-symmetric ($\langle T0, T1\rangle$, $\langle -T0, -T1\rangle$) and three-layered symmetric ($\langle T0, T1\rangle$, $\langle -T0, -T1\rangle$, $\langle T0, T1\rangle$) TSCL is considered. In both cases, $T0 \in [0, 90]^\circ$ and $T1 \in [-90, 90]^\circ$. It is noted that, some of these angles may not be feasible due to manufacturing constraints discussed earlier. However, they are presented here for qualitative discussions. The non-dimensionalized first fundamental frequency for two and three layered composites is depicted in Fig. 5. Following observations can be made for the two layered anti-symmetric laminate (see Fig. 5a):

→ the plate has maximum fundamental frequency when the fiber angle is in the range $T1 = -60^\circ$ and -45°;
→ the plate has minimum frequency when $T1 > 0$, irrespective of the angle at the center $T0$;

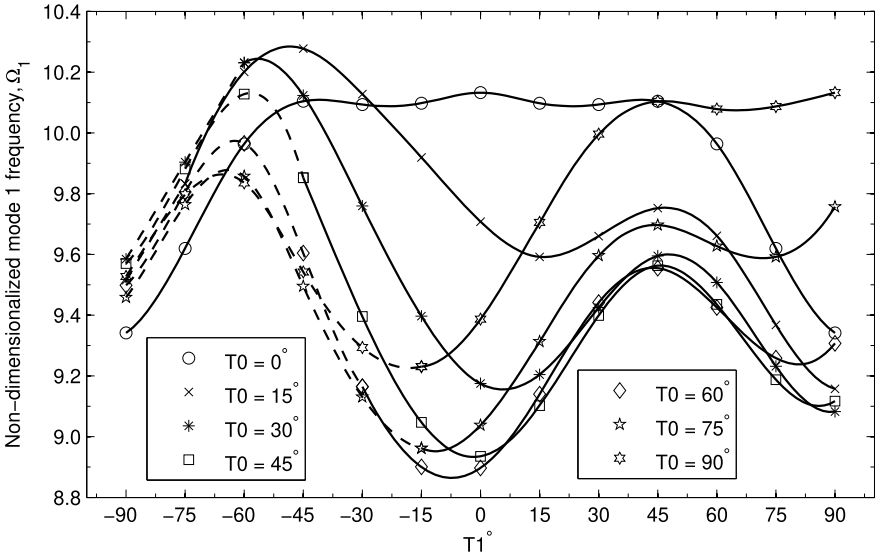

(a)

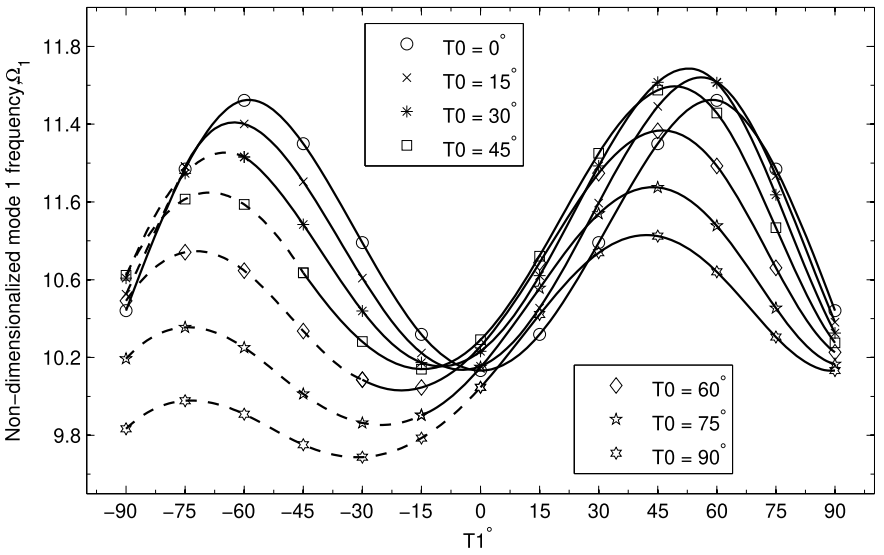

(b)

Fig. 5 Non-dimensional fundamental frequency as a function of tow-angles: **a** 2-layered anti-symmetric and **b** 3-layered symmetric tow-steered composite laminate

→ with increasing $T0$ from zero, the variation of fundamental frequency losses its symmetric with respect to $T1 = 0$;
→ the dotted lines represent the range of angles for which the constraint condition is violated.

Variation of non-dimensionalized first fundamental frequency with $T1$ for constant $T0$ for a three-layered symmetric laminate is shown in Fig. 5b. It is seen that for a particular choice of $T0$, the response of three-layered and two-layered are qualitatively similar. In this case, the maximum frequency occurs when $T1$ is $-45°$ and $60°$ for all choices of $T0$. Of all the combinations, the plate has the highest first mode frequency $\langle T0, T1\rangle = \langle 30°, 45°\rangle$. Similar to the two-layered composites, the dotted lines represent the combination of center and edge angle for which the manufacturing constraint on the curvature of the fiber is violated. It is noted that the value of the edge angle $T1$ at which the extremum frequency occurs is reversed between two and three layered composite laminates considered here.

4.2 Buckling

Next, for the two- and three- layered tow-steered composite laminate, the mechanical buckling characteristics is studied. In case of two-layered system, the layer configuration is represented by: $(\langle T0, T1\rangle, \langle -T0, -T1\rangle)$ and for three-layered symmetric the ply arrangement is as follows: $(\langle T0, T1\rangle, \langle -T0, -T1\rangle, \langle T0, T1\rangle)$. In this case, $T1$ is assumed to be between $-90°$ and $90°$ and $T0$ is varied between $0°$ and $90°$. Figure 6a shows the N_{xx}^{cr} due to mechanical forces. It is inferred that N_{xx}^{cr} is symmetric with respect to fiber edge angle ($T2 = 0$), when $T1 = 0°$, however, the symmetry is lost for other values of $T1$. The critical buckling load is maximum when center angle is $15°$ and end angle is $-60°$ and the minimum when $T1 > 0°$. Similarly,the influence of the spatial variation of the fiber angle ($T0/T1$) on the N_{xx}^{cr} for a 3-layered composite is studied. Critical buckling load numerically computed is depicted in Fig. 6b. From Fig. 6b, it is inferred that for a particular $T0$, the variation of buckling load is similar to two-layered composite. For 3-layered, the $\max(N_{xx}^{\text{cr}})$ occurs when $T1 = \pm 60°$ and $T0 = 0°$. The angles for which the manufacturing constraint is violated in shown with dashed lines in Fig. 6. For the three-layered composite laminate, the range of negatively tow-steered fiber angle $T1$, without violating the manufacturing constraint is limited, similar to the two-layered case. It is concluded that the $T1$ strongly influences the critical buckling load of the composite, irrespective of the number of layers.

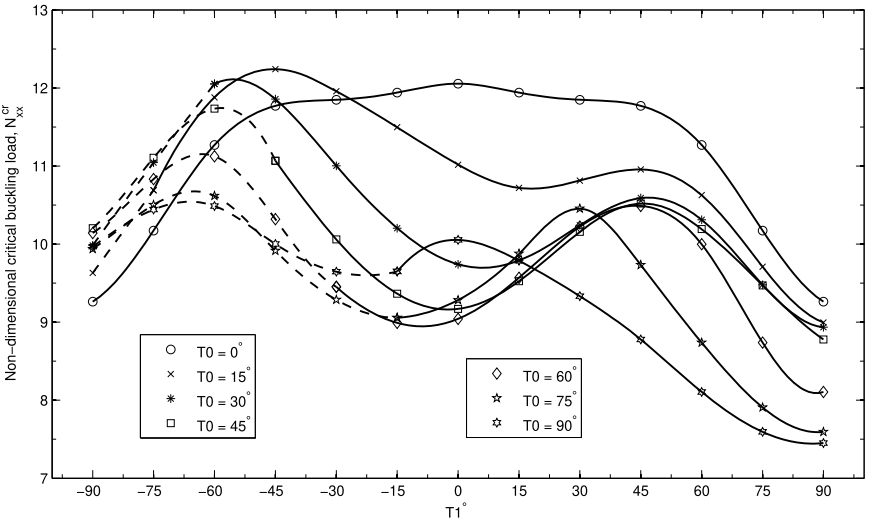

(a)

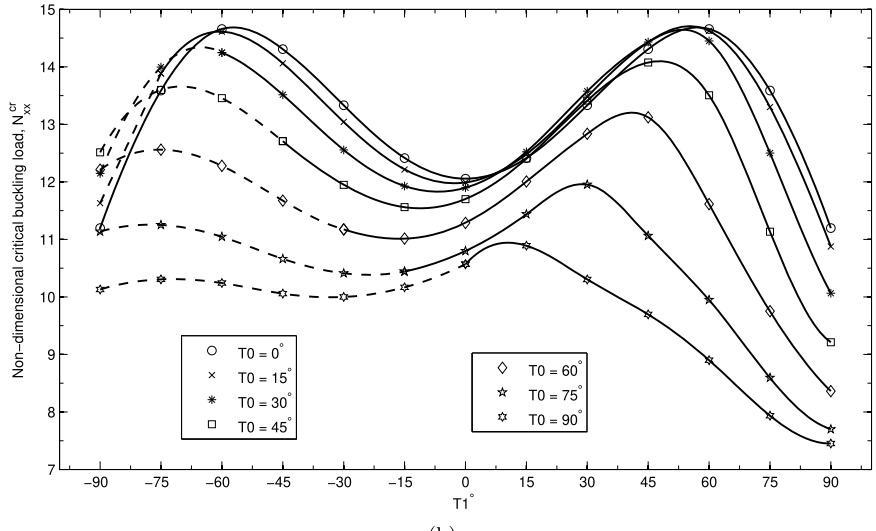

(b)

Fig. 6 Critical buckling load as a function of $T1$ for: **a** 2-layered and **b** 3-layered tow-steered composite laminates. Note that $T0 \in [0, 90]°$

4.3 Linear Flutter

Next, the aerodynamic response of tow-steered composite laminate is studied using the iso-geometric analysis framework. The plate is immersed in a supersonic flow. Although, the developed framework is general, the results are presented only for a square plate. The plate is assumed to consist of three layers with following three different ply configurations:

$$\langle 30°, 0°\rangle; \langle 45°, 90°\rangle; \langle 30°, 0°\rangle$$

$$\langle 45°, -45°\rangle, \langle -45°, -60°\rangle, \langle 0°, 45°\rangle$$

$$\langle 90°, 45°\rangle, \langle 60°, 30°\rangle, \langle 90°, 45°\rangle$$

The influence of h and the edge conditions on the critical aerodynamic pressure is also studied. Table 3 presents the effect of orientation of the fiber, plate thickness and the boundary condition on the critical aerodynamic pressure at which the plate experiences flutter and the corresponding frequency. It can be inferred that decreasing the plate thickness, the critical aerodynamic pressure increases and it is greater in case of clamped when compared to all edges simply supported, as expected. The

Table 3 Frequency—critical aerodynamic pressure for a tow-steered composite laminated for different boundary conditions and plate aspect ratios

Fiber orientation	$\frac{h}{a}$	SSSS		CCCC	
		λ_{cr}	ω_{cr} ($\times 10^4$)	λ_{cr}	ω_{cr} ($\times 10^4$)
$\langle 30°, 0°\rangle$, $\langle 45°, 90°\rangle$, $\langle 30°, 0°\rangle$	0.01	2937.69	0.6960	4145.51	1.8503
	0.02	2890.04	0.6931	3993.95	1.7842
	0.10	1931.45	0.5855	2200.98	0.9994
$\langle 45°, -45°\rangle$, $\langle -45°, -60°\rangle$, $\langle 0°, 45°\rangle$	0.01	3097.85	0.8779	4865.04	1.7863
	0.02	3045.51	0.8699	4655.66	1.7331
	0.10	2078.32	0.6986	2191.60	0.9599
$\langle 90°, 45°\rangle$, $\langle 60°, 30°\rangle$, $\langle 90°, 45°\rangle$	0.01	961.91	0.5692	1454.88	1.7307
	0.02	947.07	0.5601	1386.91	1.6345
	0.10	683.01	0.3941	515.82	1.5001

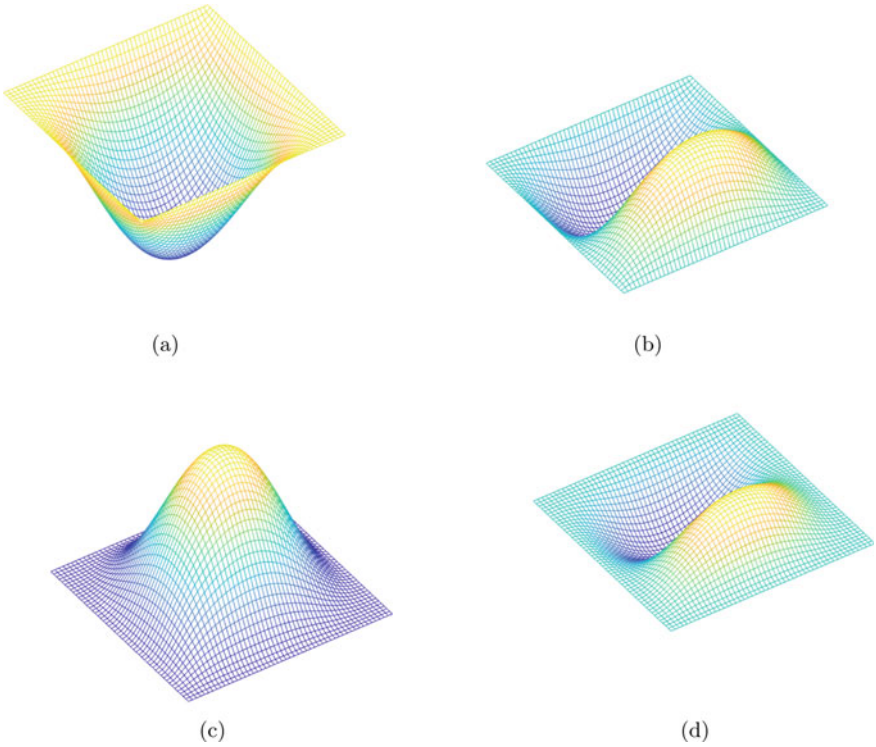

Fig. 7 First two mode shapes for: **a**–**b** simply supported and **c**–**d** fully clamped square plate with fiber orientation: $\langle 45°, -45° \rangle$, $\langle -45°, -60° \rangle$, $\langle 0°, 45° \rangle$ with $\frac{a}{h} = 100$

above observation is valid for the three different ply configurations considered. The free vibration and the flutter mode shapes for the first two fundamental frequency is shown in Figs. 7 and 8 for $h = 0.01$ and for clamped and simply supported edge conditions. The flutter mode shape is supported with the variation of frequency and critical aerodynamic pressure, depicted in Fig. 9. From Fig. 9 it is seen that with increasing pressure, the frequency increases and for a particular pressure, which is referred to as the critical aerodynamic pressure, the mode shape coalesce and the frequencies becomes complex conjugate.

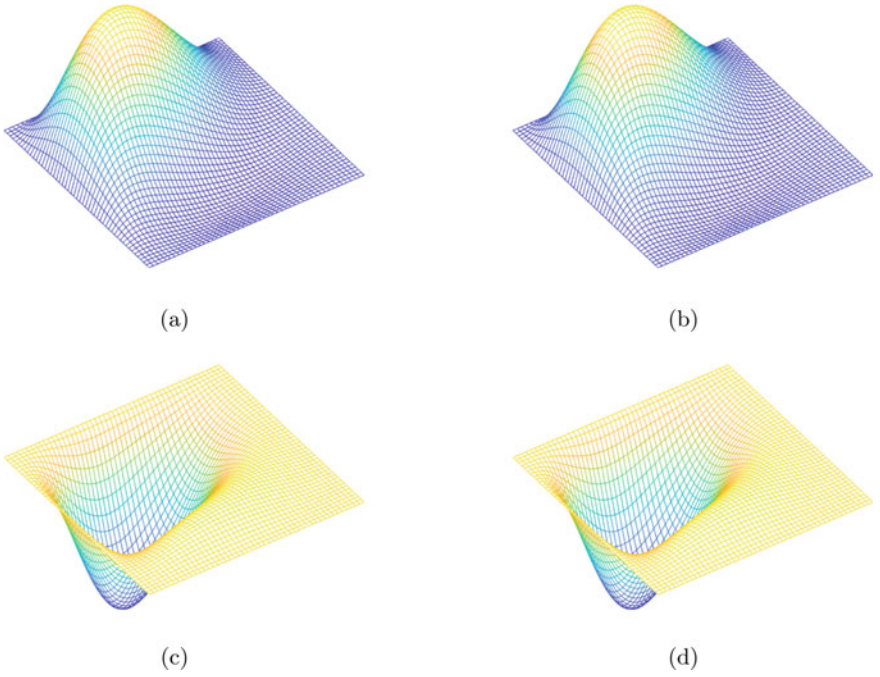

Fig. 8 Square plate immersed in a supersonic flow—mode shape for **a**–**b** all edges simply supported and **c**–**d** fully clamped plate. Plate thickness $h = 0.01$ and has three layers with fiber orientation: $\langle 45°, -45° \rangle$, $\langle -45°, -60° \rangle$, $\langle 0°, 45° \rangle$ with $\frac{a}{h} = 100$

5 Concluding Remarks

In this chapter, the free vibration, mechanical buckling and linear flutter characteristics of tow-steered composite laminate is numerically studied using an iso-geometric analysis. It is opined that the systematic parametric study done will be useful for practising designers who are interested in the design and the optimization of tow-steered laminates. Some observations are: the first fundamental frequency, buckling and flutter characteristics are strongly influenced by the spatial variation of the orientation of the fiber. The influence of increasing aspect/thickness ratio increases the fundamental frequency whilst it reduces the critical buckling load. Similar observations can be derived for the case when the plate is immersed in a supersonic flow. Due to manufacturing constraint, the practically feasible range of orientation of the fiber depends on angle at the center.

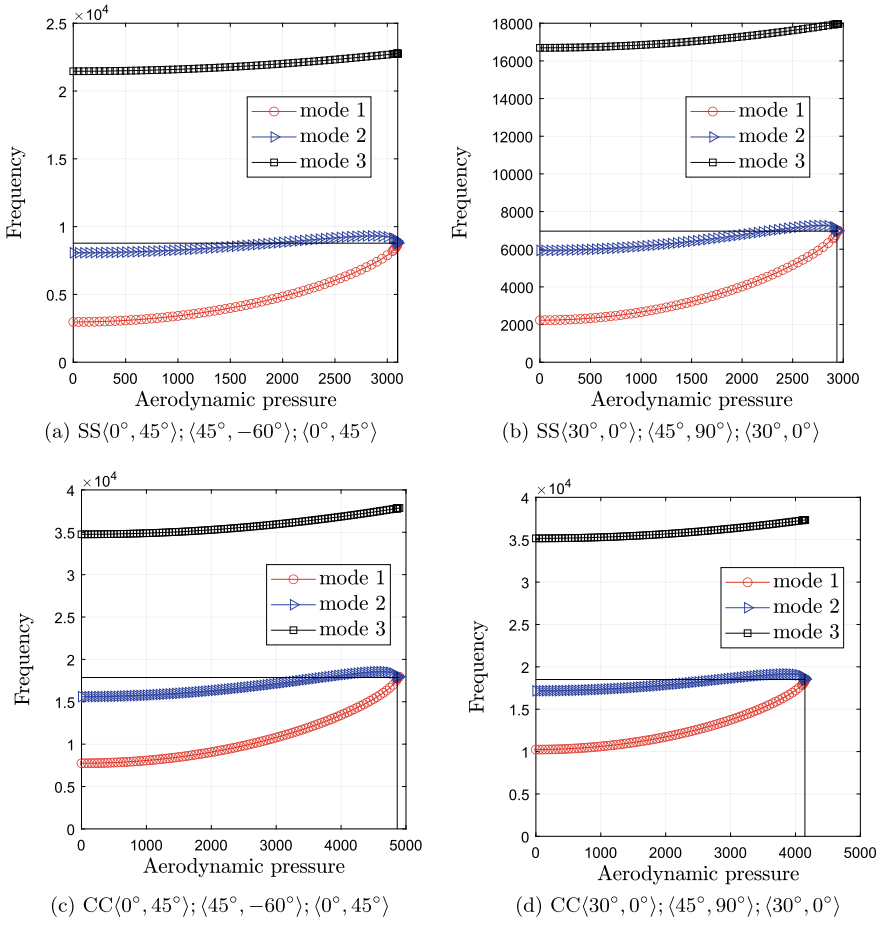

Fig. 9 Frequency-aerodynamic pressure plot for **a**–**b** full simply supported and **c**–**d** clamped square plate immersed in a supersonic flow

References

1. Altenbach H (2011) Mechanics of advanced materials for lightweight structures. Proc Inst Mech Eng Part C J Mech Eng Sci 225(11):2481–2496
2. Reddy JN (2004) Mechanics of laminated composite plates and shells: theory and analysis. CRC Press
3. Ullah H, Harland AR, Silberschmidt VV (2015) Mater Des 88:149–156
4. Wang Y, Liu X, Zhu C, Parsons A, Liu J, Huang S, Ahmed I, Rudd C, Sharmin N (2019) Production and characterisation of novel phosphate glass fibre yarns, textiles, and textile composites for biomedical applications. J Mech Behav Biomed Mater 99:47–55
5. Gurdal Z, Olmedo R (1993) In-plane response of laminates with spatially varying fiber orientations-variable stiffness concept. AIAA J 31(4):751–758
6. Hyer MW, Lee HH (1991) The use of curvilinear fiber format to improve buckling resistance of composite plates with central circular holes. Compos Struct 18(3):239–261

7. Tatting BF (1998) Analysis and design of variable stiffness composite cylinders. Ph.D. thesis. Virginia Tech
8. Wu KC, Gurdal Z (2006) Variable stiffness panel structural analyses with material nonlinearity and correlation with tests. In: 47th AIAA/ASME/ASCE/AHS/ASC structures, structural dynamics, and materials conference 14th AIAA/ASME/AHS adaptive structures conference 7th, p 2165
9. Lopes CS, Gürdal Z, Camanho PP (2008) Variable-stiffness composite panels: buckling and first-ply failure improvements over straight-fibre laminates. Comput Struct 86(9):897–907
10. Setoodeh S, Gürdal Z, Watson LT (2006) Design of variable-stiffness composite layers using cellular automata. Comput Methods Appl Mech Eng 195(9–12):836–851
11. Senocak E, Tanriover H (2007) Analysis of composite plates with variable stiffness using galerkin method. Aeronaut J 111(1118):247–255
12. Cairns DS, Mandell JF, Scott ME, Maccagnano JZ (1999) Design and manufacturing considerations for ply drops in composite structures. Compos Part B Eng 30(5):523–534
13. Her S-C (2002) Stress analysis of ply drop-off in composite structures. Compos Struct 57(1–4):235–244
14. Ribeiro P, Akhavan H, Teter A, Warmiński J (2014) A review on the mechanical behaviour of curvilinear fibre composite laminated panels. J Compos Mater 48(22):2761–2777
15. Hyer MW, Lee HH (1991) The use of curvilinear fiber format to improve buckling resistance of composite plates with central circular holes. Compos Struct 18:239–261
16. Setoodeh S, Abdalla MM, Ijsselmuiden ST, Gürdal Z (2008) Design of variable stiffness composite panels for maximum buckling load. Compos Struct 87:109–117
17. Lopes CS, Gürdal Z, Camanho PP (2010) Tailoring for strength of composite steered fibre panels with cutouts. Compos Part A Appl Sci Manufact 41:1760–1767
18. Khani A, IJsselmuiden MM, Abdalla Z, Gürdal ST (2011) Design of variable stiffness panels for maximum strength using lamination parameters. Compos Part B Eng 42:546–552
19. Abdalla MM, Gürdal Z, Abdelal GF (2009) Thermomechanical response of variable stiffness composite panels. J Therm Stress 32:187–208
20. Akhavan H, Ribeiro P (2011) Natural modes of vibration of variable stiffness composite laminates with curvilinear fibers. Compos Struct 93:3040–3047
21. Raju G, Wu Z, Kim BC, Weaver PM (2012) Prebuckling and buckling analysis of variable angle tow plates with general boundary conditions. Compos Struct 94:2961–2970
22. Raju G, Wu Z, Weaver PM (2013) Postbuckling analysis of variable angle tow plates using differential quadrature method. Compos Structs 106:74–84
23. Akhavan H, Ribeiro P, de Moura MFSF (2013) Large deflection and stresses in variable stiffness composite laminates with curvilinear fibers. Int J Mech Sci 73:14–26
24. Akhavan H, Ribeiro P, de Moura MFSF (2013) Composites laminates with linear varying fiber angles under static and dynamic loads. In: 54th AIAA/ASME/ASCE/AHS/ASC Structures, structural dynamics and materials Conference April 8–11, 2013 Boston, Massachusetts
25. Kim BC, Potter K, Weaver PM (2012) Continuous tow shearing for manufacturing variable angle tow composites. Compos Part A Appl Sci Manufact 43:1347–1356
26. Kim BC, Weaver PM, Potter K (2014) Manufacturing characteristics of the continuous tow shearing method for manufacturing of variable angle tow composites. Compos Part A Appl Sci Manufact 61:141–151
27. Falcó O, Mayugo JA, Lopes CS, Gascons N, Turon A, Costa J (2014) Variable stiffness composite panels: as-manufactured modeling and its influence on the failure behavior. Compos Part B Eng 56:660–669
28. Honda S, Narita Y (2012) Natural frequencies and vibration modes of laminated composite plates reinforced with arbitrary curvilinear fiber shape paths. J Sound Vib 331:180–191
29. Coburn BH, Wu Z, Weaver PM (2014) Buckling analysis of stiffened variable angle tow panels. Compos Struct 111:259–270
30. Natarajan S, Baiz PM, Bordas S, Rabczuk T, Kerfriden P (2011) Natural frequencies of cracked functionally graded material plates by the extended finite element method. Compos Struct 93(11):3082–3092

31. Akhavan H, Ribeiro P (2011) Natural modes of vibration of variable stiffness composite laminates with curvilinear fibers. Compos Struct 93(11):3040–3047
32. Cottrell JA, Hughes TJR, Bazilevs Y (2009) Isogeometric analysis: toward integration of CAD and FEA. Wiley
33. Nguyen VP, Simpson RN, Bordas SPA, Rabczuk T (2012) An introduction to isogeometric analysis with matlab implementation: Fem and xfem formulations, p 6. arXiv preprint arXiv:1205.2129
34. Kikuchi F, Ishii K (1999) An improved 4-node quadrilateral plate bending element of the Reissner-Mindlin type. Comput Mech 23:240–249
35. Khdeir AA, Librescu L (1988) Analysis of symmetric cross-ply elastic plates using a higher-order theory: part II: buckling and free vibration. Eur J Mech A Solids 31:259–277
36. Liew KM, Huang YQ, Reddy JN (2003) Vibration analysis of symmetrically laminated plates based on FSDT using the moving least squares differential quadrature method. Comput Methods Appl Mech Eng 192:2203–2222